Proceedings ASME Turbo Expo 2018: Turbine Technical Conference and Exposition
GT2018
June 11-15, 2018, Lillestrøm, Norway

GT2018-75460

COMPARISON OF FLAME TRANSFER FUNCTIONS MEASURED WITH LOCALLY RESOLVED FULL-FIELD-VIBROMETRY AND OH*-CHEMILUMINESCENCE

Felix Greiffenhagen, Jakob Woisetschläger
Institute for Thermal Turbomachinery and
Machine Dynamics, Graz University of Technology
8010 Graz, Austria

Johannes Gürtler, Heiko Scholz, Robert Kuschmierz, Jürgen Czarske
Technische Universität Dresden
01062 Dresden, Germany

ABSTRACT

Information about heat release can be used to discuss the flame dynamics and stability behavior of turbulent combustion systems. The most common experimental approach to determine heat release fluctuations is the recording of OH-chemiluminescence. Since there is a strong dependence of chemiluminescence on strain rate and mixture gradients, spatial information must be judged with care. As already shown in previous work, Laser Interferometric Vibrometry (LIV) directly detects the line-of-sight values of density fluctuations along the laser beam axis. Neglecting friction, losses of thermal radiation and conduction and assuming only small fluctuations of pressure in the reaction zone, heat release fluctuations can be calculated directly from density fluctuations. With available LIV techniques only pointwise scanning was feasible, resulting in time-consuming traversing of the flame to cover the whole flame field. A new camera-based full-field-LIV-system, developed at Technische Universität Dresden, is capable to simultaneously determine spatial information of heat release within the whole field with only one measurement, lasting a few minutes. This leads to a dramatical reduction of measurement time and furthermore reduces experimental efforts. Since the system is able to measure the complete flame at once, it is also possible to get information about the transient behavior of the combustion process. In this work the full-field-LIV system was applied for the first time on a swirl stabilized, lean and premixed methane flame. The results of this newly developed technique were checked against those of a commercially available single-beam LIV-system. Finally, the flame transfer function (FTF) was recorded with full-field-LIV and OH*-chemiluminescence and compared against each other.*

NOMENCLATURE

c	[m/s]	speed of sound
CTA		constant temperature anemometry
f	[Hz]	frequency
Δf	[Hz]	Doppler frequency
f_B	[Hz]	Bragg frequency
G	[m³/kg]	Gladstone-Dale constant
FFT		fast Fourier transform
FTF		flame transfer function
h	[J/kg]	enthalpy
k_{vib}	[mm/s/V]	vibrometer calibration constant
I	[W/m²]	intensity of the laser beam
L	[m]	optical path
LIV		laser interferometric vibrometry
n	[]	refractive index
p	[Pa]	pressure
p'	[Pa]	pressure fluctuation
$\mathbf{q}$	[W/m²]	heat flux
q'_v	[J/m³]	volumetric heat release fluctuation
PM		photomultiplier
SNR		signal to noise ratio
t	[s]	time
T	[K]	temperature
u	[m/s]	velocity
U	[V]	LIV output voltage
Y	[]	mass fraction
κ	[]	heat capacity ratio
λ	[nm]	laser wave-length
ρ	[kg/m³]	density
ρ'	[kg/m³]	density fluctuation
τ_{ij}	[N/m²]	viscous stress tensor
Φ	[]	equivalence ratio
$\Delta\varphi$	[°]	phase difference

INTRODUCTION

Combustion noise generated by fluctuations of heat release is not only a pollutant but also leads to combustion instabilities, which in worst case can lead to malfunction or damage of turbomachinery. In aero-engines, improvements of fan, compressor and turbine led to a reduction of noise level, which puts the focus more and more on noise generated by unsteady combustion. Contrary to this, modern combustion concepts with lean and premixed flames, targeting towards lower temperature and therefore low NOx, are more vulnerable to instabilities [1], caused by reduced core mass flow and damping capabilities. Swirl stabilized flames, used in modern combustion concepts, tend to react nonlinear to incoming perturbations [2] from the fuel or air path. Experimental approaches to determine those fluctuations are mostly done with CH* or OH* radical chemiluminescence or by planar laser induced fluorescence (P-LIF). Balachandran et al. [3] state, that global heat release can be obtained from chemiluminescence recordings when investigating premixed flames. Lauer [4] recommended to carefully interpret chemiluminescence data, especially local resolved data should be taken with care, since mixture gradients and strain rate influence the local emission of radicals.

The unsteadiness of heat release leads to fluctuations of density in the flame zone. Laser interferometric vibrometers directly record line-of-sight integrated density fluctuations along the laser beam axis in unconfined [5] [6], as well as in confined flames [7]. By using tomographic algorithms, it is possible to derive local data. Recently it was shown, that LIV is capable to predict density fluctuations quantitatively [8]. A not yet published work from the authors of this paper also showed good agreement in a quantitative comparison between amplitude and phase of the global heat release, obtained from chemiluminescence recordings and LIV data [9].

Up to now, commercially available LIV-systems were used, originally designed to measure surface vibrations without mechanical contact. Those LIVs are only capable to measure in a single position through the flow field (line-of-sight technique). To get full-field data, time consuming traversing of the flame is necessary. This can last up to several hours, which may lead to problems if the combustion system is not stable for such a long measurement period. To overcome this, the target of the Austrian-German joint research project "Full-field laser vibrometry for combustion diagnostics" funded by the Austrian FWF and the German DFG is to develop a planar, camera based full-field-LIV-system. This system should be capable to record the whole combustion field within a single measurement, by forming interference pattern between an object- and a reference beam on a high speed camera. Compared to a single detector, a full-field-LIV has a spatial resolution dependent on the resolution of the image sensor of the camera. Also the recording of unsteady data over the whole flame field is possible. To demonstrate the capability of such a system with a resolution of 110x110 pixels, a flame-transfer-function (FTF) was recorded for a flame published recently [10].

MATERIALS AND METHODS

Relating heat release and density fluctuations

Fluctuations of density in a reacting flow are caused by several mechanisms which may occur in any combination. The focus in this work was on the calculation of heat release fluctuations from interferometrical measurements of density fluctuations in an unconfined flame. Since this method measures a summation of all present effects altering density and no separation is possible, a discussion of all influences and their order of magnitude on the data obtained from LIV has to be done. Starting with the energy equation, neglecting body forces [11] [12] and considering a reactive gas, consisting of N species [13], the energy equation can be written in terms of density fluctuations [12]:

$$\frac{d\rho}{dt} = \frac{1}{c^2}\frac{dp}{dt} + \frac{(\kappa-1)\rho}{\kappa p}\left\{\sum_{n=1}^{N}\frac{\partial h}{\partial Y_n}\bigg|_{T,p,Y_m}\rho\frac{dY_n}{dt} - \rho\frac{\partial h}{\partial \rho}\bigg|_{p,Y_n}\left(\sum_{n=1}^{N}\frac{\partial \rho}{\partial Y_n}\bigg|_{T,p,Y_m}\frac{dY_n}{dt}\right) + \nabla\mathbf{q} - \frac{\partial u_i}{\partial x_j}\tau_{ij}\right\} \quad (1)$$

With κ the ratio of heat capacities, ρ as density, c the speed of sound, pressure p and Y_n the mass fraction of the nth species. The first term on the right side describes the influence of changes of pressure on density. It has already been shown, that pressure changes caused by sound waves or turbulence can be visualized in a non-reacting flow by interferometric measurements [14] [15] [16]. The term $\rho\frac{dY_n}{dt} = \omega_n - \nabla \boldsymbol{J_n}$ in the first summation is equal to the production of the nth species ω_n minus its flux by diffusion $\nabla \boldsymbol{J_n}$. When diffusion is neglected, the first summation on the right side describes the rate of heat release per unit volume $-q_v$ due to chemical reaction. The expression Y_m with $Y_m \neq n$ means, that there is no contribution from other molecules in each summation loop. The second summation term describes the change of density due to changes of species concentration at constant temperature and pressure. When burning hydrocarbons with air, this term is small compared to the heat release and therefore can be neglected, since the average molar mass is nearly constant [12], caused by the dilution of the reactive species with inert nitrogen [11]. This term has to be considered, if a fuel is burned with pure oxygen. $\nabla\mathbf{q}$ represents the heat flux due to conduction, convection and radiation. The last part $\frac{\partial u_i}{\partial x_j}\tau_{ij}$, with τ_{ij}, the viscous stress tensor and the flow velocities u_i defines the heat addition from friction.

When measuring density fluctuations, caused by combustion of hydrocarbons with air, the following equation considers all influence on the fluctuations measured:

$$\frac{d\rho}{dt} = \frac{1}{c^2}\frac{dp}{dt} + \frac{(\kappa-1)\rho}{\kappa p}\left\{\sum_{n=1}^{N}\frac{\partial h}{\partial Y_n}\bigg|_{T,p,Y_m}\rho\frac{dY_n}{dt} + \nabla\mathbf{q} - \frac{\partial u_i}{\partial x_j}\tau_{ij}\right\} \quad (2)$$

The results presented in this work are based on the assumption, that all fluctuations detected by LIV were caused by heat release fluctuations. To estimate the influence of other effects, experiments were undertaken which are presented here in a short version. A detailed discussion will be published soon in [9].

In a first attempt, a vibrometer was used to measure fluctuations 5mm downstream of the unconfined combustor exit without flame but with the same operation point used for all investigations in this work. The flow was siren excited at a frequency of 212Hz, with a mean flow velocity of approximately 5m/s. In this configuration, the density fluctuations detected, were caused by turbulence and noise (pressure term) and heat addition from friction in the flow (stress tensor term). Later, the flame was ignited and the same position was measured again. The amplitude of the LIV output at the excitation frequency without flame was 425 times smaller than that with combustion. Besides the excitation frequency the amplitudes measured were even smaller. Additionally it has to be considered, that the heat release fluctuations at this positions were relatively small compared to high fluctuating positions (~factor 4), whereas the fluctuations of the flow were very high at this position. Since all investigations were done with an unconfined flame, no thermoacoustic resonance could occur and it was shown the contribution of the fluctuations caused by aerodynamics were very small compared to that of heat release fluctuations. Also the sound field surrounding the flame was measured via LIV. The resulting amplitudes of the pressure waves, caused by unsteady combustion, where approximately 10^4 times smaller than that in the flame. Microphone measurements in a distance of 0.3m, recorded a sound pressure level of 70dB at 212Hz. The $\nabla\mathbf{q}$ term, which sums up the heat loses due to conduction and radiation, can be addressed as the highest uncertainty, since it is the hardest one to quantify. Since no confinement was used for the investigations presented here, conduction was neglected. To quantify the total power of radiation, a thermopile (Kipp&Zonen CA2) was used to measure the radiation from 0.2-50µm, resulting in an overall value of approximately 180W which is 5.2% of the total thermal power of 3.44kW. Due to the thermal inertia of the thermopile, no frequency resolved measurement of the thermal radian was possible but it has to be considered that approximately 5% of heat release fluctuations are not detected by LIV. Being aware of the influences on density fluctuations, the flame and its surrounding could be separated in three different zones. In the flame the following equation can be used:

$$\frac{d\rho'_{flame}}{dt} = -\frac{(\kappa-1)\rho}{\kappa p}\frac{dq'_v}{dt} \quad (3)$$

With $\frac{dq'_v}{dt}$, the volumetric heat release fluctuations and $\frac{d\rho'_{flame}}{dt}$ the density fluctuations detect by LIV in the flame. Downstream of the flame, with no chemical reaction, density fluctuations are mainly caused by convection of heat, since the amplitudes are much smaller compared to that in the reaction zone, pressure fluctuations contribute to the density fluctuations too. In this region, the density fluctuations can be described as:

$$\frac{d\rho'}{dt} = \frac{1}{c^2}\frac{dp'}{dt} + \frac{(\kappa-1)\rho}{\kappa p}\nabla\mathbf{q} \quad (4)$$

In the surrounding of the flame, where no reaction and no convection of heat occurs, density changes are mainly caused by sound waves.

$$\frac{d\rho'}{dt} = \frac{1}{c^2}\frac{dp'}{dt} \quad (5)$$

In the present work all measurements were performed in the flame and therefore the quantitative values of heat release fluctuations were calculated according to (3). While LIV directly records $\frac{d\rho'}{dt}$, it was also necessary to know local absolute density, the local ratio of heat capacities, which is a function of temperature and species concentration (equivalence ratio) and pressure, later it can be seen, that the local equivalence ratio is also necessary for the calculation of density fluctuations from the refractive index fluctuation data recorded by LIV. The first was obtained from shearography (differential interferometry) measurements [17] [18]. This measurement technique, in short words, measures the instantaneous refractive index or density gradient along a defined direction. By summing up the gradients from an undisturbed area with ambient density, to the center of the flame, the local absolute density can be calculated. With the ideal gas law, temperature was calculated from density. Although the global equivalence ratio can be calculated easily from the fuel and air mass flows, the local and phase resolved distribution was measured via OH*/CH* chemiluminescence [19] [4], recorded with an image enhanced camera. Since air and methane were already premixed before entering the combustor, only slight periodical fluctuations of equivalence ratio were observed, resulting in a mean equivalence ratio of 0.7. Since the exact gas composition in the measurement area was not known, a mean value of the ratio of heat capacities between cold reactants and hot products was calculated (Table 1). In a worst case, the deviation of the term $\frac{(\kappa-1)}{\kappa}$ between reactants and products was in a range between five and six percent. Considering all the corrections of local constants discussed above, very good agreement between quantitative data from LIV measurements and OH*-chemiluminescence, recorded with a photomultiplier (PM) and an image enhanced camera were achieved ([9] to be submitted), when applied to the same flame investigated here. The total power of heat release fluctuations measured with PM was 155W, the image enhanced camera resulted in a value of 153W while the result obtained from LIV was 151W. The phase between heat release fluctuation and trigger signal at the perturbation frequency of 212Hz was 132° for the photomultiplier and 129° for the integral LIV phase, the image enhanced camera resulted in a phase angle of 122°. Also the comparison of sound power calculated from LIV-recorded density fluctuations and the sound power measured with microphones showed good agreement [8].

Laser Interferometric Vibrometry

When passing through any fluid, light interacts with the molecules present, resulting in a delayed wave front, compared to that of an undisturbed propagation of light. This change of the speed of light does not only dependent on the medium itself but also on its density [20]. Whereby the refractive index n correlates the ratio of speed of light in vacuum to that in a medium. With a species depended factor, the Gladstone-Dale constant G, density can be calculated whenever the refractive index is known from measurements:

$$n(x,y,z,t) - 1 = \rho(x,y,z,t)\, G \tag{6}$$

LIV is a line-of-sight measurement, meaning the quantity n is integrated along the laser beam axis:

$$L(t) = \int_l n(x,y,z,t)\, dz \tag{7}$$

with L the optical path. This sampling laser beam, or object beam is reflected back into the LIV by a mirror after passing through the flame twice. By interfering the object beam and an internal reference beam, as can be seen on the bottom left part of Figure 1, LIVs detect changes of the optical path L. The intensity pattern seen on the detector is a function of the phase difference $\Delta\varphi$ between object and reference beam, which can be related to the variation of the optical path, e.g. by density fluctuations, the following way [21]:

$$I(\Delta L) = \frac{I_0}{2}(1 + \cos(\Delta\varphi)) = \frac{I_0}{2}\left(1 + \cos\left(2\pi\frac{\Delta L}{\lambda}\right)\right) \tag{8}$$

The LIV principle uses a frequency modulation f_B by acousto-optical modulators (Bragg-cells) in the reference beam. So, without any changes in optical path, the interference pattern is modulated by this carrier frequency:

$$I(f_B, t) = \frac{I_0}{2}(1 + \cos(2\pi(f_B)t) \tag{9}$$

When the optical path changes, these fluctuations in optical path modulate the carrier frequency. This modulation frequency can be expressed as $\pm\Delta f = \frac{2u}{\lambda}$ (Doppler-effect) where u is the "velocity" of the object (or dL/dt) including a factor two, since the beam passes the flame twice. Now (8) changes to

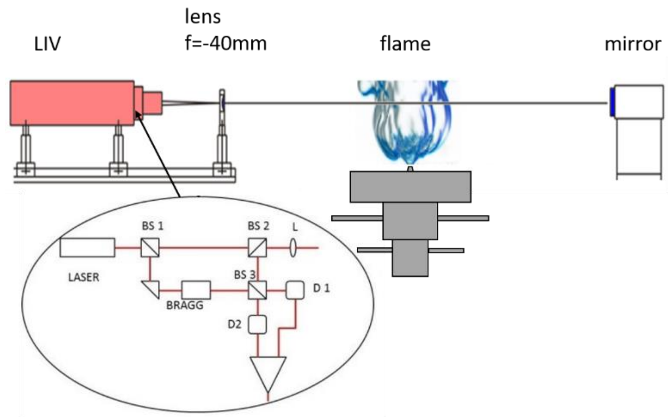

Figure 1: Measurement setup for single point LIV measurements; the laser beam is collimated by a -40mm lens, passing the flame and mirrored back. Internally the object beam is interfered with a reference beam to detect changes of the optical path. Bottom: principle function of LIV: BS… beam splitter, L… lens, D… detector, BRAGG... acousto-optical modulator

$$I(\Delta f, t) = \frac{I_0}{2}(1 + \cos(2\pi(f_B \pm \Delta f)t) \tag{10}$$

The sign of the Doppler shift is determined by the direction of velocity.

In this configuration it is possible to detect surface vibrations or refractive index (density) changes with respect to their sign or direction of motion with sub-nanometer resolution [22]. Using commercially available vibrometers, the change of optical path can be directly calculated from the output voltage of the LIV-system with the calibration factor k_{vib} in mm/s/V.

$$\frac{dL'}{dt} = \frac{d}{dt}\int_l n'(x,y,z,t) = k_{vib}U(t) \tag{11}$$

With the apostrophe indicating the fluctuation component. The application of LIV can be found in: [5], [23], [24].

In the single-laser-beam setup, the laser beam was collimated to a diameter of 2mm with a -40mm lens and reflected with a mirror, passing the measurement zone twice. The LIV (interferometer head OF-503, velocity decoder OFV-5000, calibration factor 2mm/s/V, 100kHz bandwidth, no filters, Polytec, Waldbronn, Germany) was kept at a fixed position, while the flame was traversed with a measurement grid of 2mm, to scan the whole flame (Figure 1). In total 16 positions were measured in lateral direction and 58 points in height, resulting in an overall number of 928 measurement points. Each point was scanned for 30 seconds. Data acquisition was performed NI-9121 input modules and LabView 2012 software, with a sample rate of 16384 samples per second.

Since the flame shows axisymmetric behavior [10] when looking at time averaged data, only half of the flame was scanned,

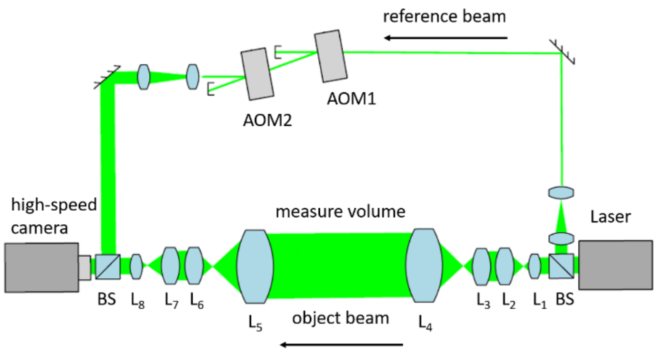

Figure 2: Camera based LIV in a transmissive setup: the laser beam is split up into an object beam and a reference beam (BS beam splitter). The reference beam is guided around the flame and modulated with acousto-optical modulators (AOM 1,2), while the object beam is expanded with a lens system (L1-L4) and bundled again (L5-L8) after the measure volume. Both beams interfere at the image sensor of a high-speed camera, forming a 110x110 array of single Laser Vibrometers on the pixel sensor.

resulting in a field with a size of 114x30mm. If axial symmetry is given, local data can be calculated using Abel inversion, otherwise tomographic reconstruction from different projections of the flame would have been necessary. Time resolved recordings with an image enhanced camera at 212Hz showed, that not all structures developed axisymmetric but when looking at time averaged recordings symmetry was given. In this work only time averaged data was used but problems were found at other siren frequencies.

When relating the refractive index to density with the Gladstone-Dale constant in a reactive medium, one has to take care about the influence of the species concentrations on G. The Gladstone-Dale constant in general is only weakly dispersive and not dependent on temperature or pressure but on the type of species and its individual mass fraction. This means, that especially in non-premixed combustion, where equivalence ratio waves can occur, the local and time resolved equivalence ratio Φ in the reaction zone has to be known to calculate a local Gladstone-Dale constant. As described above the OH*/CH* chemiluminescence was recorded with an image enhanced camera.

Since air and methane were already premixed before entering the combustor, only slight periodical fluctuations of equivalence ratio were observed. The combustion zone showed a stable equivalence ratio field with a mean value of 0.7. Therefore the field of view was divided into three-zones with different Gladstone-Dale constants, using a mean value between reactants and products in the combustion zone with $G = 2.5.10^{-4}$m³/kg a linear transition area and an area were no combustion occurs, assuming air with a humidity of 50% with $G = 2.23.10^{-4}$m³/kg. The values for the Gladstone-Dale constant were calculated using data from Gardiner et al. [25] and GASEQ software.

ϕ [ ]	**0.6**	**0.7**	**0.8**
$G_{react.\ 300K}$ [m³/kg]	2.51E-04	2.55E-04	2.58E-04
$G_{prod.\ 1500K}$ [m³/kg]	2.43E-04	2.45E-04	2.47E-04
$G_{average}$ [m³/kg]	2.47E-04	2.50E-04	2.53E-04
$G_{deviation}$ [%]	1.7	2.0	2.2
$\kappa - 1/\kappa\rvert_{react.\ 300K}$ [ ]	0.281	0.281	0.281
$\kappa - 1/\kappa\rvert_{prod.\ 1500K}$ [ ]	0.249	0.247	0.246
$\kappa - 1/\kappa\rvert_{average}$ [ ]	0.265	0.265	0.263
$\kappa - 1/\kappa\rvert_{deviation}$ [%]	5.6	5.8	6.1

Table 1: Gladstone-Dale constants of reactants and products at the corresponding temperatures: only slight dependency on the equivalence ratio, for post processing an average G between reactants and products was used. Bottom: temperature and species dependency of the right side of (3), again a mean value was used for further calculations

CAMERA BASED FULL-FIELD-LIV

Scanning the whole combustion field with high resolution is time consuming and requires stability of the flame for long periods. One possibility to shorten measurement time is to expand the laser beam to a diameter corresponding the flame size and measure the whole field at once. Practically this leads to a bad SNR and furthermore local information is lost.

To avoid these problems, a high-speed camera based LIV-system (full-field-LIV) has been in development [26]. The main working principle is the same as described above. The laser beam was expanded with a lens system (Figure 2) to a diameter of 71mm to form the object beam. After passing the measurement volume (flame) it was bundled again with a further lens system (lenses 5 to 8 in Figure 2). The reference beam was guided around the flame at save distance, so that no influence of the flame on the reference beam could occur. In the reference beam two acousto-optical modulators introduced the carrier frequency. After a beam splitter, both beams interfered at a high-speed camera (Phantom v1610, Vision Research) with a frame rate of 200kHz and a resolution of 110x110 pixel, resulting in a spatial resolution of 50x50 mm. Due to the high data rate, the total measurement time of 27s was divided into three measurements with nine seconds each, the maximum the high speed camera is able to record at once. To ease alignment and reduce losses and cross-talk between the pixels due to refraction by the density gradients in the flame, the system was set up in transmission with the laser beam passing the measurement volume only once. Thus, with a collimated lens system as shown in Figure 2, a change of angle in the beam path caused by refraction, led to a change of angle on the image sensor, but not to a change of position on the sensor, avoiding cross-talk between the pixels. Besides the dramatically reduction of measurement time, the instantaneous measurement of the whole field offers another advantage. As shown by Hampel et al. [27], cross-correlation

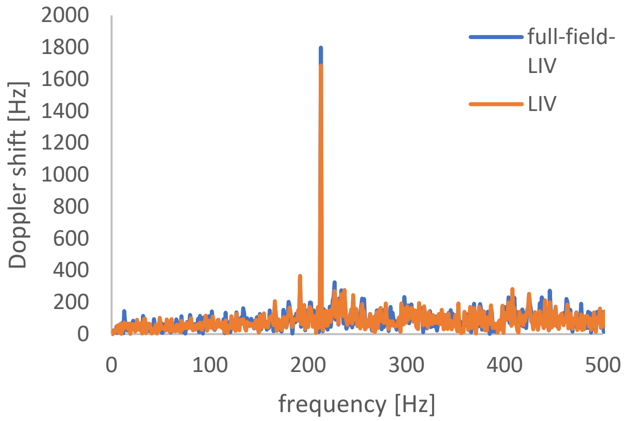

Figure 4: Comparison of the Doppler shift amplitude spectra in the flame between full-field-LIV and LIV. Both measurements were done simultaneously and at the same position: the high peak at 212Hz is caused by the excitation of the flame by the siren. A slightly higher amplitude was observed for the full-field-LIV system due to a smaller measurement area and therefore less spatial averaging

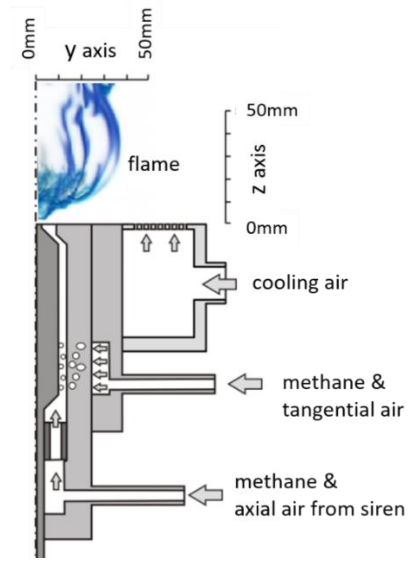

Figure 3: Working principle of the unconfined methane burner: tangential and axial air were mixed with methane far upstream to ensure a homogeneous mixture; the axial airflow was modulated with a rotating disc (siren) shortly before entering the combustor to force a defined perturbation of the flame

between two vibrometer signals can be used to determine spatial and temporal coherent structures in the flow. This can be done by calculating the phase angles of the complex cross correlation spectrum between the pixel signals or between pixel signal and time reference (siren).
From heat release fluctuations and velocity measurements, the flame transfer function (FTF) can be determined.
Finally, the planar measurement also makes it possible to analyze the unsteady behavior of the whole combustion zone, when looking at the time resolved data recorded.

LIV signal processing

The comparison of data recorded by a single point LIV and the full-field-LIV was done using a siren to perturb the flame, at 212Hz for a good signal-to-noise ratio. To record the FTF the flame was excited at various frequency, again with the siren. All post processing was done in MATLAB 2015a. Fast Fourier transformations were calculated using MATLABs built in FFT code pwelch and cross correlation spectra between camera pixel signals and siren were obtained from the also implemented function cpsd [28], [29]. Single point LIV data was recorded with a sample rate of 16384S/s and evaluated with a sample length of 163840 samples with no window functions, resulting in a frequency resolution of 0.1Hz with three spectra averaged. All measurements showed a high peak at the perturbation frequency with only low amplitudes in the side bins and therefore only small scalloping losses. The amplitudes obtained from the circular shaped laser beam, were corrected to a square shape, by multiplying the value of each measure position with a correction factor. With this square shaped measure grid, it was possible to cover the whole combustion field.
The full-field-LIV used a 200kHz sampling rate for the time signals, after demodulation of the carrier frequency superimposed by the AOMs. The phase angle of each measuring position was obtained from a cross correlation between the LIV signal and the siren trigger. Total quantities were calculated by summing up all positions with respect to their phase angles.
The FFT and cross-correlations for the full-field LIV were done with the same algorithms as described above used for the single point LIV but with a sample length of 200kS, resulting in a frequency resolution of 1Hz. As described above, for the correction of temperature, density and the Gladstone-Dale constant, an Abel inversion is necessary, which can only be done on one half of the symmetric flame. This made it necessary to average both sides. The evaluation of the heat release fluctuations were done on this averaged half, all plots of full-field-LIV data show this averaged half, although the whole flame was recorded.
After an Abel inversion of the line-of-sight data, a Gladstone-Dale correction with three zones was performed, to relate changes in refractive index to changes in density. Also a correction of the local density and ratio of heat capacities was done for the local data fields, according to the local temperature, measured with differential interferometry, and equivalence ratio, measured with OH*/CH* chemiluminescence [9].

The flame transfer function

Flame transfer functions (FTF) correlate the relative fluctuations of heat release rate in the total flame volume ($\dot{Q}'/\bar{\dot{Q}}$) and the relative velocity fluctuations ($v'/\bar{v}$) at the burner outlet and are used for the characterization of flames. While the total heat release fluctuations $\dot{Q}'$ were recorded by full-field-LIV or by OH*-chemiluminescence (photomultiplier PMM01, Thorlabs

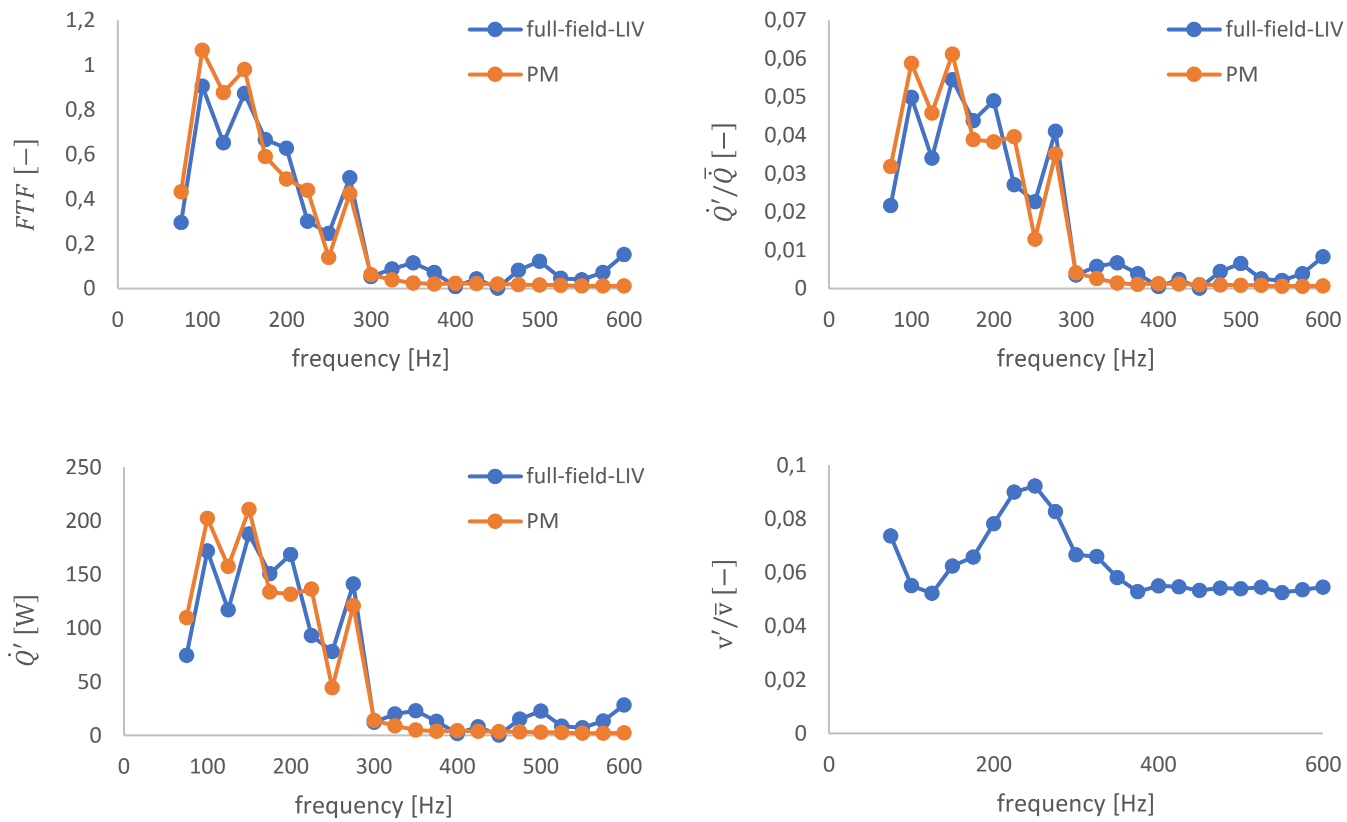

Figure 5 top left: Flame transfer function recorded with full-field-LIV and PM, with flame excitation from 75Hz to 600Hz in steps of 25Hz; top right: heat release fluctuations relative to mean heat release, full-field-LIV vs. PM; bottom left: global heat release fluctuations full-field-LIV vs. PM; bottom right: velocity fluctuations relative to mean velocity at burner exit, recorded at the cold flow with constant temperature anemometry

Inc. with OH* filter 310±3nm CWL, FWHM 10±2nm Edmund Optics), the velocity recordings were done with three-component Constant Temperature Anemometry (CTA, Dantec Dynamics) 7mm above the burner outlet nozzle and 7mm shifted radial to the burner axis. The CTA measurements were done without flame. The FTF was sampled in steps of 25Hz between 75Hz and 600Hz by these three measurement techniques. The mean heat release was calculated from the fuel mass flow, assuming complete combustion.

The swirl-stabilized atmospheric methane burner

All measurements were performed on an unconfined swirl-stabilized, methane-fired burner at ambient conditions. The working principle of this burner is documented in detail by Giuliani et al. [30]. As shown by Peterleithner et al. [10] the flame shows axisymmetric behavior without perturbation. Therefore it was possible to derive local data via Abel inversion from the line-of-sight data recorded with LIV.

In Figure 3 the experimental configuration of the burner can be seen. To prevent any fluctuations of equivalence ratio caused by changes of mass flow, both axial and tangential air were already mixed with methane far upstream, to ensure a homogenous mixture. The axial airflow was forced into axial direction with a stratifier. While the tangential air entered the plenum trough 32 cylindrical bores aligned tangentially and symmetrical around the burner z-axis, generating a simplified swirl number of 0.52. Assuming complete combustion, the burner had a thermal power of 3.44kW and a mean equivalence ratio of 0.7 - measured via OH*/CH* chemiluminescence. In the configuration described above, the flame stayed detached approximately 20mm above the from the burner exit nozzle a stable way. As long as the combustor is fired with premixed air/fuel and no confinement, it showed a slight natural resonance around 230Hz, as can be seen in the $v'/\bar{v}$ graph in Figure 5, where the flow showed a strong response to incoming perturbations close to this frequency.

Fuel and air mass flow rate were determined using caloric mass flow meters of the EL-FLOW series from Bronkhorst, Netherlands, with an accuracy of 0.6% full scale.

To ensure repeatability of the experiment and high SNRs the axial air/fuel mass flow was modulated with a siren [31] shortly before entering the combustor. The flame showed a good response at a siren frequency of 212Hz, resulting in strong perturbations of the flame and a corresponding sharp peak of heat release fluctuations at this frequency. The working principle of the siren can be described by a rotating sprocket with equally

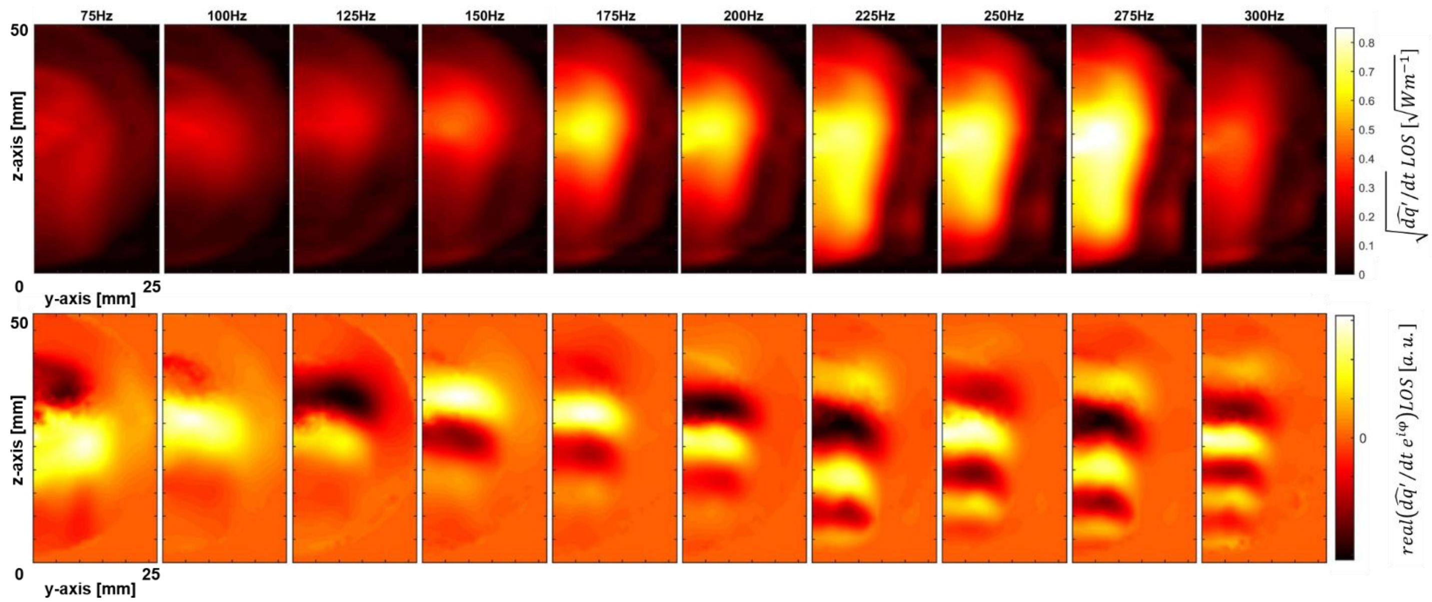

Figure 6 top: Square root of averaged line-of-sight heat release fluctuations, recorded with full-field-LIV; bottom: real part of the complex heat release fluctuation amplitude, phase information was obtained from a cross correlation between full-field-LIV and siren trigger

distributed teeth, blocking or releasing the full cross section area of the axial mass flow at the frequency chosen.
For the single-point-LIV system scanning was necessary. This was done by traversing (lightweight traverse, Dantec Dynamics) the flame with the LIV systems in a fixed position, while a photomultiplier moved with the system.

RESULTS AND DISCUSSION

Comparison between LIV and full-field-LIV

To quantitatively compare the results obtained from full-field-LIV with those from single point LIV, a single position in the flame was measured at y=10mm and z=15mm with the standard LIV and the new system simultaneously. The flame was excited at a frequency of 212Hz. Figure 4 shows a comparison between the amplitude spectra of the Doppler frequency shift (eq. (10)) of both LIV-systems. Since the absolute value of heat release or density fluctuation in the volume measured is depend on the laser beam diameter, which was different for the single point LIV and the full-field-LIV, this representation was chosen. As can be seen, the results agreed very well. At the perturbation frequency the deviation between the results is approximately 6%, with a higher value recorded with the full-field-LIV system. This can be explained by the difference in the beam diameters. The standard LIV beam was collimated to a diameter of 2mm, resulting in a measurement area of 3,14mm², while the corresponding measurement area of the full-field-system was approximately 0.22mm². Due to the larger beam diameter of the single point LIV laser beam, a larger area was averaged and therefore high local peaks were smoothed.

Flame Transfer Function: full-field-LIV vs. photomultiplier

The focus of this work mainly laid on a first test of a newly developed measurement device for accurate global and local data of heat release fluctuations in highly turbulent flames. Because of this, the results section mostly concentrates on the difference between the results obtained from full-field-LIV and OH*-chemiluminescence.
The FTFs were recorded by incrementing the siren frequency in steps of 25Hz from 75Hz to 600Hz. Data from full-field-LIV and photomultiplier (PM) with OH*-filter was recorded simultaneously with a recording length of 3x9s. Splitting into three parts was necessary, since the maximum recording length of the high-speed camera was nine seconds at a frame rate of 200kHz. The heat release fluctuations obtained from full field-LIV were calculated as described above. To get $\dot{Q}'$ from OH*-chemiluminescence recordings, complete combustion was assumed and the total thermal power was normalized with the mean intensity counts from the PM recordings, a [W/OH*count] scaling was calculated.
Figure 5 shows the FTFs, total heat release fluctuations and the corresponding velocity fluctuations from 75 to 600Hz. When looking at the graphs, it can be seen, that the fluctuations obtained from full-field-LIV showed the same tendencies as the OH*-chemiluminescence data up to 300Hz. With two exceptions: at 200Hz an increase of the amplitude was calculated from full-field-LIV recordings, whereas the PM showed a slight decrease. At 225Hz the PM measurements showed a slight increase of amplitude, while the full-field-LIV measured a decrease. In this region, from 75 to 300Hz, the deviation between the total amplitudes was between 10% and 70% in the worst case

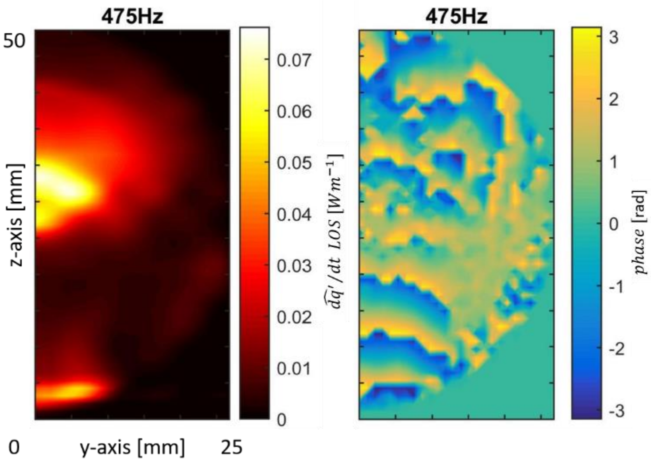

Figure 7 left: Line-of-sight density fluctuation amplitudes at 474Hz siren frequency; right: corresponding phase, obtained from a cross correlation between full-field-LIV and siren trigger, downstream the phase information got lost due to a bad SNR and therefore wrong integral values were calculated

at 250Hz. Several explanations were found for these deviations, when looking at local data. The top line in Figure 6 shows the square root of the local amplitude of heat release fluctuations. Since the amplitudes differed in more than one order of magnitude, a normalization with a square root was used, in order to apply the same scaling for all images. As can be seen, a circular shaped masking of the interferograms obtained from full-field-LIV was necessary. This was caused by the poor interference contrast between the object beam and the reference beam, which were interfered at the high-speed camera sensor, in the corner regions. Additionally it can be seen, that the measurement field was too small to capture all the fluctuations. Recording done with an image enhanced camera and OH*-filter showed, that the OH*-chemiluminescence reached up to nearly 120mm, while the recordings done with the full-field-LIV where limited to a size of 50mm x 50mm, caused by the size of the optics used. The quantitative comparison between OH*-chemiluminescence and single-point-LIV at a siren frequency of 212Hz, as described above [9], resulted in a deviation of 2.6% in amplitude and 2.3% in phase. The single-point-LIV field reached up to 119mm in axial direction and 30mm in radial direction. But the main uncertainty for accurate calculations was found somewhere else. To compute the heat release fluctuations from density fluctuations, the local absolute density has to be known (equation (3)). For the investigations presented in this work, the local temperature/density field for a siren perturbation frequency of 212Hz was available.

In a next step, the full-field-LIV system should be capable to measure not only density fluctuations but simultaneously recording the density field. This will lead to accurate and easier quantitative measurements of heat release fluctuations, since no second measurement technique has to be applied.

Another uncertainty was the symmetry of the flame. Since local temperature/density and equivalence ratio were necessary for the correct calculation of heat release from density fluctuations, all corrections had to be done for local full-field-LIV data. The line-of-sight data was averaged between the right and the left side of the measurement field and then transformed to local data by means of Abel inversion, which is only valid for radial symmetry of the time-averaged measurements. When checking the symmetry, it was found that the symmetry was in between 85 to 105%, dependent on the siren frequency. For future work, the measurement of different projections and tomographic reconstruction should be considered, since the measurement time itself is very short with this new full-field-LIV system.

Up to 300Hz siren perturbation OH*-chemiluminescence and full-field-LIV mostly followed the same trend, at higher frequencies, up to 600Hz, it was hard to find similarities. Except for two points at 400 and 450Hz, the fluctuations calculated from full-field-LIV data led to higher values than those of the OH*chemiluminescence. Since the full-field-LIV measures the amplitudes of density fluctuations at certain positions, local phase information is necessary to calculate the total fluctuations by summing up all measurement position with their corresponding phase. The phase was calculated from a cross-correlation between full-field-LIV and the siren trigger. At high siren frequencies, starting at 350Hz the local phase information downstream was lost due to bad SNR (Figure 7).

This led to regions with a nearly constant or chaotic phase and therefore too high values of the total heat release fluctuations. In an investigation done by Peterleithner et al. [7], in which the laser beam of the single-point-LIV was expanded to a diameter corresponding the flame size, a similar trend was found. Also the heat release fluctuations recorded by LIV showed higher values at high siren frequencies compared to those recorded by OH*-chemiluminescence.

To get information about the local fluctuations with respect to their phase, the bottom line of Figure 6 shows the real part of the complex local amplitude, including phase information. Since the amplitudes at different siren frequencies differed in more than one order of magnitude, an individual scaling was chosen for each image, so that the phases can be seen clearly. When looking at the total heat release fluctuations in Figure 5, it can be seen, that the integral values of 75 and 100Hz were high, although the local values in top of Figure 6 seemed to be low compared to higher frequencies. This behavior can be explained by the axial extension of one period of fluctuations, which can be seen in the bottom line of Figure 6. At low frequencies, approximately half of a period of fluctuations fitted in the axial length of the flame, acting more or less like a monopole. If one full period or a multiple thereof fitted in the axial length of the flame, the local amplitudes began to cancel out each other, when integrating over the whole measurement field. This can be seen at 250Hz, were approximately two periods with relatively constant local peak amplitudes led to a small global amplitude, although the local peak amplitudes (Figure 6 top), were of high values. At 275Hz very high local values at approximately 30mm in z-direction led to a high integral value, since the local amplitudes of the fluctuations upstream were too low to dampen the integral fluctuation.

CONCLUSION

Heat release fluctuations were recorded with a newly developed full-field-LIV and OH*-chemiluminescence. While chemiluminescence recordings were done integral over the whole flame, the full-field-LIV recordings were done with a line-of-sight measurement grid of 0.22mm² per pixel and summed up later, with respect to their local phase. The mean velocity and velocity fluctuations were recorded with constant temperature anemometry in the cold flow. To quantify the results of the newly developed system, a comparison of a single position in the flame was recorded simultaneously with the full-field-LIV and a standard LIV. The results of both systems agreed well in frequency and amplitude. When looking at the local data of the full-field-LIV, it was found, that the measurement field, with a size of 50mm x 50mm, was too small to record the whole flame zone. Also it was necessary to mask the corner regions of the full-field-LIV recordings due to a bad SNR. This can be solved by expanding the laser beam to a larger diameter. The strongest influence on the quantitative measurement of heat release fluctuations was found to be the local absolute density/temperature. Additionally, an axial shift of the flame at different siren frequencies led to problems in finding the corresponding axial position of the absolute density/temperature field. Also the imperfect axial symmetry of the flame, which had to be assumed to calculate local data with Abel inversion from one two dimensional projection, caused uncertainties. Tomographic reconstruction from different projections could solve this problem.

Besides the problems describe above, one has to consider, that this was the first attempt of the application of this newly developed full-field-LIV system to a swirl stabilized flame. Overall the results agreed well to that obtained from OH*-chemiluminescence qualitatively at most of the siren frequencies. Additionally to the integral data, this measurement methodology records local data with high resolution. The setup combines 110x110 vibrometers in one single measurement. Assuming a recording time of 30 seconds, one measurement period with full-field-LIV lasts 30 seconds, while scanning the whole field with a single point LIV would last more than 100 hours, excluding traversing time. Since the whole field is recorded simultaneously, a correlation between single pixels can be used to calculate line-of-sight velocity of coherent structures in the field. Further investigations aim towards a calculation of the mean density field from full-field-LIV measurements to solve to problems described above. In the future full-field-LIV should be capable to combine the recording of heat release fluctuations, line-of-sight velocity and mean density in one single measurement, offering a powerful tool for experimental combustion diagnostics.

ACKNOWLEDGMENTS

This research was funded by the Austrian Science Fund FWF within Grant No. FWF-I2544-N30 and the Deutsche Forschungsgemeinschaft within grant DFG CZ 55/33-1. This project is a Lead-Agency D-A-CH project between Graz University of Technology, Austria, and Technische Universität Dresden, Germany. with the title "Full-field laser vibrometry for combustion diagnostics".

We also thank Mr. Sterzinger and Mr. Wachter for their support in the operation of the CTA-system.

REFERENCES

[1] A. P. Dowling und Y. Mahmoudi, „Combustion noise," *Proceedings of the Combustion Institute,* Bd. 35, pp. 65-100, 2015.

[2] S. Candel, D. Durox, T. Schuller, J. .. Bourgouin und J. P. Moeck, Dynamics of swirling flames, Bd. 46, 2014, pp. 147-173.

[3] R. Balachandran, B. O. Ayoola, C. Kaminski, A. P. Dowling und E. Mastorakos, „Experimental investigation of the nonlinear response of turbulent premixed flames to imposed inlet velocity oscillations," Bd. 143, pp. 37-55, 10 2005.

[4] M. R. W. Lauer, Determination of the Heat Release Distribution in Turbulent Flames by Chemi-luminescence Imaging, Technische Universität München, 2011, pp. 147-173.

[5] T. Leitgeb, T. Schuller, D. Durox, F. Giuliani, S. Köberl und J. Woisetschläger, „Interferometric determination of heat release rate in a pulsated flame," *Combustion and Flame,* Bd. 160, pp. 589-600, 2013.

[6] F. Giuliani, B. Wagner, J. Woisetschlaeger und F. Heitmeir, „Laser vibrometry for real-time combustion instability diagnostics," in *Proc. ASME Turbo Expo*, 2006.

[7] J. Peterleithner, N. V. Stadlmair, J. Woisetschläger und T. Sattelmayer, „Analysis of measured flame transfer functions with locally resolved density fluctuation and OH-Chemiluminescence Data," *Journal of Engineering for Gas Turbines and Power,* Bd. 138, 2016.

[8] F. Greiffenhagen, J. Peterleithner und J. Woisetschläger, „Prediction of Combustion Noise from a Swirl-Stabilized Flame using Laser-Interferometric-Vibrometry validated by Acoustic Measurements," in *Proceedings of the ASME Turbo Expo*, 2017.

[9] F. Greiffenhagen, J. Peterleithner, J. Gürtler, A. Fischer, J. Woisetschläger und J. Czarske, „Discussion of laser interferometric vibrometry for the determination of heat release fluctuations in an unconfined swirl-stabilized flame," *Combustion and Flame,* 2017.

[10] J. Peterleithner, F. Salcher und J. Woisetschläger, „Frequency resolved interferometric detection of local density fluctuations in flames," *Proc. 17th International Symposium on Application of Laser Techniques to Fluid Mechanics, Lisbon,,* 2014.

[11] T. C. Lieuwen, Unsteady combustor physics, Cambridge, : Cambridge Univ. Press, 2012, pp. XIX, 405 S..

[12] D. G. Crighton, A. P. Dowling, J. E. F. Williams, M. A. Heckl und F. A. Leppington, Modern Methods in

Analytical Acoustics: Lecture Notes, Springer London, 1996.

[13] F. A. Williams, Combustion Theory, WESTVIEW PR, 1994.

[14] P. Gren, K. Tatar, J. Granström, N.-E. Molin und E. V. Jansson, „Laser vibrometry measurements of vibration and sound fields of a bowed violin," *Measurement Science and Technology,* Bd. 17, pp. 635-644, 2006.

[15] L. Zipser, S. Lindner und R. Behrendt, „Interferometric Measurement and Visualisation of Acoustic Waves and Vortexes," Bd. 69, pp. 275-281, 01 2002.

[16] N. Mayrhofer und J. Woisetschlaeger, „Frequency analysis of turbulent compressible flows by laser vibrometry," *Experiments in Fluids,* Bd. 21, pp. 153-161, 2001.

[17] G. Pretzler, H. Jäger und T. Neger, „High-accuracy differential interferometry for the investigation of phase objects," *Measurement Science and Technology,* Bd. 4, pp. 649-658, 1993.

[18] M. Hipp, P. Reiterer, J. Woisetschläger, H. Philipp, G. Pretzler, W. Fliesser und T. Neger, „Application of interferometric fringe evaluation software at Technical University Graz," *Proceedings of SPIE - The International Society for Optical Engineering,* Bd. 3745, pp. 281-292, 1999.

[19] C. S. Panoutsos, Y. Hardalupas und A. M. K. P. Taylor, „Numerical evaluation of equivalence ratio measurement using OH* and CH* chemiluminescence in premixed and non-premixed methane-air flames," *Combustion and Flame,* Bd. 156, pp. 273-291, 2009.

[20] W. Merzkirch, Flow Visualization, 2 Hrsg., Academic Press,Orlando, San Diego, New York, Austin, Boston, London, Sydney, Tokyo, Toronto, 1987.

[21] A. a. M. F. a. S. H. Lewin, „Heterodyn-Interferometer zur Vibrationsanalyse," *Technisches Messen,* Bd. 57, p. 335–345, 1990.

[22] A. C. Lewin, *Compact laser vibrometer for industrial and medical applications,* Bd. 3411, 1998, pp. 61-67.

[23] J. Li, D. Durox, F. Richecoeur und T. Schuller, „Analysis of chemiluminescence, density and heat release rate fluctuations in acoustically perturbed laminar premixed flames," *Combustion and Flame,* Bd. 162, pp. 3934-3945, 2015.

[24] J. Peterleithner und J. Woisetschläger, „Laser vibrometry for combustion diagnostics in thermoacoustic research," *Technisches Messen,* Bd. 82, pp. 549-555, 2015.

[25] W. C. Gardiner, Y. Hidaka und T. Tanzawa, „Refractivity of Combustion Gases," *Combustion and Flame,* Bd. 40, pp. 213-219, 1981.

[26] J. Gürtler, F. Greiffenhagen, J. Woisetschläger, D. Haufe und J. Czarske, „Non-invasive seedingless measurements of the flame transfer function using high-speed camera-based laser vibrometry," in *Proc. SPIE 10329*, 2017.

[27] B. Hampel und J. Woisetschläger, „Frequency- and space-resolved measurement of local density fluctuations in air by laser vibrometry," *Measurement Science and Technology,* Bd. 17, pp. 2835-2842, 2006.

[28] G. Heinzel, A. Rüdiger und R. Schilling, *Spectrum and spectral density estimation by the Discrete Fourier transform (DFT), including a comprehensive list of window functions and some new at-top windows,* 2002.

[29] A. V. Oppenheim und R. W. Schafer, Digital signal processing, Englewood Cliffs, N.J.: Prentice-Hall., 1975.

[30] F. Giuliani, J. W. Woisetschläger und T. Leitgeb, „Design and validation of a burner with variable geometry for extended combustion range," in *Proceedings of the ASME Turbo Expo, GT2012-68236*, 2012.

[31] F. Giuliani, A. Lang, K. Johannes Gradl, P. Siebenhofer und J. Fritzer, „Air flow modulation for refined control of the combustion dynamics using a novel actuator," *Journal of Engineering for Gas Turbines and Power,* Bd. 134, 2012.

[32] G. Pretzler, H. Jäger, T. Neger, H. Philipp und J. Woisetschlaeger, „Comparison of Different Methods of Abel Inversion Using Computer Simulated and Experimental Side-On Data," *Zeitschrift für Naturforsch.,* Bd. 47a, pp. 955-970, 1992.

